NR/SBR/Organoclay Nanocomposites: Effects of Molecular Interactions Upon the Clay Microstructure and Mechano-Dynamic Properties

Mitra Tavakoli,[1] Ali Asghar Katbab,[2] Hossein Nazockdast[2]

[1]*Department of Textile Engineering, Yazd University, Yazd, Iran*
[2]*Department of Polymer Engineering and Color Technology, Amirkabir University of Technology, Tehran, Iran*

Received 4 September 2010; accepted 12 April 2011
DOI 10.1002/app.34673
Published online 22 August 2011 in Wiley Online Library (wileyonlinelibrary.com).

ABSTRACT: Nanocomposites based on (70/30) blends of natural rubber (NR), styrene-butadiene rubber (SBR), and organoclay (OC) have been prepared successfully via melt-mixing process. Effects of the extent of polymers/clay interactions upon the developed microstructure, fatigue life, and dynamic energy loss by the nanocomposites have been investigated. Maleated EPDM (EPDM-*g*-MAH) and epoxidized NR (ENR50) were employed as compatibilizer. Nanocomposites were characterized by means of X-ray diffractometer (XRD), transmission electron microscope (TEM), scanning electron microscope, atomic force microscopy, root mean square, and dynamic mechanical thermal analysis. EPDM-*g*-MAH showed more potential in enhancing dispersion of the clay nanolayers and their interaction with rubber phases. More potential for separating and dispersing the clay nanoplatelets with better interface enhancement was exhibited by EPDM-*g*-MAH as compatibilizer. This was consistent with higher resistance towards large strain cyclic deformations along with more heat build-up characteristics showed by EPDM-*g*-MAH based nanocomposites especially at compatibilizer/organoclay ratio of 3. Pronounced non-terminal behavior within low frequency region was also observed for melt storage modulus of this nanocomposite, indicating higher extent of intercalation/exfoliation microstructure with reinforced interfaces than the nanocomposite generated by ENR50. © 2011 Wiley Periodicals, Inc. J Appl Polym Sci 123: 1853–1864, 2012

Key words: blend; microstructure; organoclay; nanocomposites; rubber

INTRODUCTION

Reinforcement of polymers by the clay filler have long been attracting great interests because of possible nano dispersion of the clay silicate layers, and hence enhancement of the polymer/filler interaction at low filler loading.[1–3]

Incorporation of surface active fillers into the elastomeric materials has been known as an important tool to reduce the entropic resistance (nerve) of the rubber chains during melt processing as well as reinforcing various technical properties of the final product. The potential of filler in improving the processability and mechano-dynamic properties of an elastomeric material is mainly governed by the extent of interaction within the interface of polymer segments and surface of the filler particles as well as the state of filler dispersion.[4]

Silicate layers of nanoclay with a high aspect ratio which can provide high interacting surfaces to the adjacent polymer segments are stacked by weak van der-Waals forces so that polymer chains are able to intercalate into the gallery spaces between the nanolayers. The extent of intercalation and dispersion state of nanolayers depends on the *d*-spacing, and degree of affinity of the polymer matrix to interact with clay tactoids. When the clay particles are mixed with a polymer matrix, three types of microstructures can be obtained, including: immisible micro composite in which clay tactoids are only dispersed throughout the matrix without nanoscale interaction with the polymer segments, intercalated and exfoliated nanostructures. In intercalated state, the polymer chains are inserted into gallery spaces of the nanoclay particles, leading to the expansion of the gap between platelets.[5,6] To obtain the exfoliated microstructure, nanolayers should be separated and dispersed uniformly throughout the polymer matrix. The primary aim in preparing polymer/clay nanocomposites is to attain a very high degree of dispersion of clay nanolayers which can provide large surface areas, leading to a significant improvement in physical, mechanical, and thermal properties compared with the virgin polymer.[7]

Organophilic modification of nanoclay by organic treatments not only makes the clay tactoids more compatible with the organic polymers but also results in increasing the spacing between the nanolayers.[8] It should be noted that direct melt intercalation of

Correspondence to: A. A. Katbab (katbab@aut.ac.ir).

polymer in organosilicates is primarily driven by the enthalpic interactions, therefore the fully exfoliation of the silicate layers hardly occurs.[9,10] To achieve improved clay dispersion and hence enhanced properties, the compatibility between the hydrophobic polymer chains and surface of the organoclay (OC) is essential by incorporation of a suitable compatibilizer.[11,12] Bousmina[13] and Dennis et al.[14] have also reported that a balance between diffusion process and the applied mechanical stress during mixing should be established to obtain high level of exfoliation throughout the molten matrix. However, longer residence time and sufficient shear intensity during mixing process are needed when polymer-filler compatibility is not strong enough.[15]

Polymer blending has been used as an effective approach to modify the shortcomings of the neat polymers.[16] Although many polymer blends have been reported as miscible systems,[17] most polymer pairs are incompatible and show coarse morphology and need to be compatibilized by a suitable material, leading to the improvement of compatibility and interfacial adhesion between the blend components.[18] Such compatibilizers can be incorporated in the form of block or graft copolymers or functionalized polymeric materials.

Recently, several articles have been published on preparation, characterization, and properties of rubber/clay nanocomposites.[19–21] In most of the works, a solution mixing method has been used for preparing polymer/clay nanocomposites.[22–24] However, from the commercial and environmental points of view, the melt intercalation process is preferred. Not many articles have centered on preparing rubber/clay nanocomposites by melt compounding[25–27] especially when the rubber matrix is in the form of a binary blend of two different rubbers.[28–30] It has been shown that partitioning of the clay particles in an immiscible rubber–rubber blend is mainly governed by the nature of the rubber phases, their melt viscosity difference during mixing process, and the organophilic treatment of the nanoclay.[31–33]

Blend of natural rubber (NR) and styrene-butadiene rubber (SBR) has widely been used in tire industries to optimize the compound processability with the required mechano-dynamic properties. NR is known to exhibit numerous outstanding properties, such as low hysteresis, high resilience, excellent fatigue resistance, and high strength. NR/OC nanocomposites have attracted great interests in recent years[34–38] as well as SBR/OC nanocomposites.[39,40] To the best of our knowledge, less research works exist to address nanocomposites based on compatibilized hybrid NR/SBR blends and OC prepared via the melt-mixing process, dealing with the effects of extent of molecular interactions between rubber phases and clay particles upon the nanocomposite microstructure, and properties of the corresponding vulcanizates. Teh et al.[41–43] and Rajasekar et al.[44] have carried out research works using epoxidized NR (ENR50) as compatibilizer for NR/OC rubber nanocomposites. Effectiveness of maleic anhydride grafted ethylene-propylene-diene rubber (EPDM-*g*-MAH) as compatibilizer for NR/OC nanocomposite has been investigated and reported in our previous paper.[45]

In the present article, attempts have been made for the first time to evaluate the influence of the type and level of interfacial compatibilization upon the degree of molecular interaction between the rubber phases and the clay particles, and hence the developed microstructure in NR/SBR/OC nanocomposites prepared by melt-mixing process. For this purpose, EPDM-*g*-MAH and epoxidized NR type ENR50 were employed. Distribution of clay nanolayers in the two rubber phases and their dispersion state as well as extent of molecular interaction with the blend components have been evaluated by performing TEM, DMTA analysis, and melt dynamic rheometry. Moreover, the characteristics of the prepared blend nanocomposites under large strain dynamic deformation have been studied via measuring fatigue life and heat generation characteristic of the prepared nanocomposite vulcanizates.

EXPERIMENTAL

Materials

A commercial NR, SLR-20 product of Aroma rubber manufactures (Sri-Lanka) with the Mooney viscosity of 73.5 (ML(1 + 4) at 100°C), styrene-butadiene rubber (SBR-1502 with 23.5% styrene) product of JSC Togliatti kauchuck (Russian Federation) with the Mooney viscosity of 54.9 (ML(1 + 4) at 100°C), EPDM-*g*-MAH (OPTIM P-635) with a graft percentage of 0.4 wt %, was supplied by Pluss polymers (New Delhi, India) and ENR50 was purchased from San-Thap International (Bangkok, Thailand). Compounding ingredients including, sulfur (S), zinc oxide (ZnO), stearic acid and *N*-cyclo hexyl-2-benzothiazyl sulfenamide (CBS) were commercial grade products and used as-received. A modified OC, Cloisite 15A, (ditallow dimethyl ammonium salts of bentonite) supplied by Southern clay (USA) products was used to prepare nanocomposite samples.

Compounding and preparation of samples

Melt compounding was performed in a banbury type internal mixer model Brabender 350E (Germany). To achieve high level of interaction between rubber phases and clay particles, two-step mixing was employed. Mixing was started at a low

TABLE I
Compositions of the Different Prepared Compounds

Sample code[a]	Clay content (% wt)	Compatibilizer type	Compatibilizer/clay (wt/wt)
B	–	–	–
B4	4	–	–
B4EN1	4	ENR50	1
B4EP1	4	EPDM-*g*-MAH	1
B4EN2	4	ENR50	2
B4EP2	4	EPDM-*g*-MAH	2
B4EN3	4	ENR50	3
B4EP3	4	EPDM-*g*-MAH	3
BEN2	–	ENR50	–
BEP2	–	EPDM-*g*-MAH	–

[a] "B" means blend of NR and SBR.

rotor speed (40 rpm), and then mixing speed was raised to 90 rpm to apply more intense shearing on the swollen clay particles. For this purpose, rubber phases and then compatibilizer were first fed into the mixer at the starting temperature of 70°C and mixing was continued till the torque reached the stationary level. OC was then fed and mixing was continued at 40 rpm for 12 min, and then mixing speed was increased to 90 rpm. The final mixes were discharged by the overall time of 20 min. Curatives were added into the as-prepared compounds in a Brabender laboratory size two-roll mill model PM300 (Germany) at 40–50°C for 4–5 min. The OC concentration was kept constant at 4 wt % and compatibilizer to OC weight ratio was varied by the values of 1, 2, and 3. The composition of the used curing system was 1.5 phr stearic acid, 5 phr zinc oxide, 1.3 phr CBS, and 2.2 phr sulfur. All the prepared NR/SBR based composites along with their codings are described in Table I.

Characterization

The extent of intercalation of nanoclay particles by the rubber phases was evaluated using X-ray diffractometer model Philips Expert diffractometer (The Netherlands) with Cu Kα radiation (wave length, $\lambda = 0.154$ nm) and a tube voltage of 40 kV with the current of 40 mA. Bragg's law, defined as $\lambda = 2d\sin\theta$ was used to compute the crystallographic spacing (d-spacing) for OC and nanocomposites. The samples were scanned with the rate of 0.02 s^{-1} between $2\theta = 1$–$12°$.

The microstructure and clay dispersion state were examined with a Tecnai^{TM} G^2 F30 (FEI Company) high performance transmission electron microscope applying an acceleration voltage of 300 kV. For this purpose, ultra-thin cross-sections (less than 100 nm) of the specimens were prepared by using a Leica EM FC6 ultra microtome equipped with a diamond knife at approximately −100°C using liquid nitrogen.

Fractured surfaces of the vulcanizates were also studied using scanning electron microscope (SEM), Philips, model XL30 (The Netherlands) operated at an accelerating voltage of 30 kV. A thin layer of gold was deposited on the fractured surfaces of the samples to prevent electrostatic charging during examination, using a sputter coater, BAL-TEC, model SCD005 (Swiss).

Atomic force microscopic (AFM) analysis was also performed on the samples using the AFM instrument Dualscope/Rasterscope C26, DME (Denmark). Surface scanning and analysis of the samples were carried out at ambient conditions using tapping mode probes with constant amplitude and resonance frequency of 190 kHz. Height images were recorded at the resonance frequency of the cantilever. The measurement of the mean roughness (arithmetic average), R_a, and the root mean square (RMS) roughness calculation[46] were done for the same size of scan area for comparison purpose.

Storage modulus (E') and the dynamic loss factor (tan δ) as a function of temperature were assessed for the vulcanized samples by performing dynamic mechanical thermal analysis (DMTA) using a DMA-Triton, model Tritec 2000 (England). DMTA spectra were taken in tension mode at 1 Hz frequency in a broad temperature range of −100 to + 100°C.

To obtain more information of the nanocomposites microstructure and dispersion state of clay nanoplatelets, dynamic melt rheometry was performed on the uncured samples using a Paar Physica US200 rheometrics mechanical spectrometer (RMS) (Austria) with a set of 25 mm diameter parallel plates at 160°C. The strain amplitude was selected within the linear viscoelastic region (1%), by performing a strain sweep test on the samples, and samples were frequency swept within the frequency region of 0.01–1000 rad/s. Variation of complex viscosity (η*) and elastic modulus (G') was recorded.

Curing characteristics of the prepared compounds were evaluated at 155°C according to the ASTM 5289 standard using a rubber curing rheometer. Effects of the presence of nanoclay particles and compatibilizer molecules upon curing parameters including scorch time (t_2), optimum cure time (t_{90}), maximum and minimum torque (M_H, M_L) and also cure rate index were investigated. The cure rate index (CRI) was obtained based on the difference between optimum cure and scorch time ($100/(t_{90} - t_2)$).

Tensile properties of the samples were studied by performing tensile test on the vulcanizates according to the ASTM 412-93 test method. For this purpose, all compounds were vulcanized at 155°C into sheets with the thickness of 2 mm in a hydraulic compression hot press, model Dr. Collin, P200P (Germany). The vulcanized sheets were cut into dumbbell-shaped specimens and then tested by using a tensile testing machine with a cross head speed of 500 mm/min.

Fatigue life of the vulcanized samples was evaluated by using Monsanto Fatigue to Failure Tester operating at 100 rpm and the extension ratio of 1.7. For this purpose, five test specimens were used for each composite vulcanizate and the number of cycles required to break the test piece was recorded automatically on the equipment. The average fatigue life (N) of each sample was computed by using the Japan Industrial Standard formula.[47]

Heat generation behavior of the samples under cyclic deformation was studied according to the standard ASTM D-3182 by means of a Goodrich flexometer, model Doli Ultimate Flexometer (Germany). The test pieces were kept at initial temperature of 50°C and test frequency of 1800 cycles/min. The temperature rise of the samples was followed within the period of 30 min.

RESULTS AND DISCUSSION

Microstructure characterization

Figure 1 displays the XRD patterns of the pristine OC along with XRD of both uncompatibilized and samples compatibilized by ENR50, and EPDM-*g*-MAH. The neat Cloisite15A showed an intense diffraction peak at around $2\theta = 2.734°$, corresponding to the basal spacing (001 plane) of 3.22 nm. It is observed that the clay diffraction peaks in the structure of the uncompatibilized NR/SBR/clay composite (B4) has slightly shifted to the lower angles, implying the occurrence of intercalation of clay galleries by the elastomer phases though not significant. Moreover, two other peaks at higher angles are also visible in the XRD pattern of the neat Cloisite15A, indicating the presence of higher orders for the clay nanolayers. These are attributed to the d_{002} and d_{003} clay galleries which are weakly modified by the clay surface modifier.[45] Therefore, diffusion of the rubber chains into these two small spacings can hardly occur. However, increasing the content of either ENR50 or EPDM-*g*-MAH in the formulation of the blend composites not only reduced the intensity of the d_{001} peak, but also led to the displacement of this peak to lower diffraction angle, indicating enhancement of interaction between rubber phases and clay tactoids. As can be observed in this figure, the main diffraction peak ($2\theta = 2.734°$) has almost disappeared in the XRD spectra of B4EP3 and B4EN3 nanocomposites, implying high disordered dispersion of the clay platelets throughout the blend matrix. Nevertheless, to further verify the extent of the OC dispersion in NR/SBR matrix, TEM examination was carried out on B4, B4EP3, and B4EN3 samples.

TEM photomicrographs of the two separately prepared NR/SBR/OC blend nanocomposite vulcanizates compatibilized with the two EPDM-*g*-MAH and ENR50 (compatibilizer/clay = 3) along with

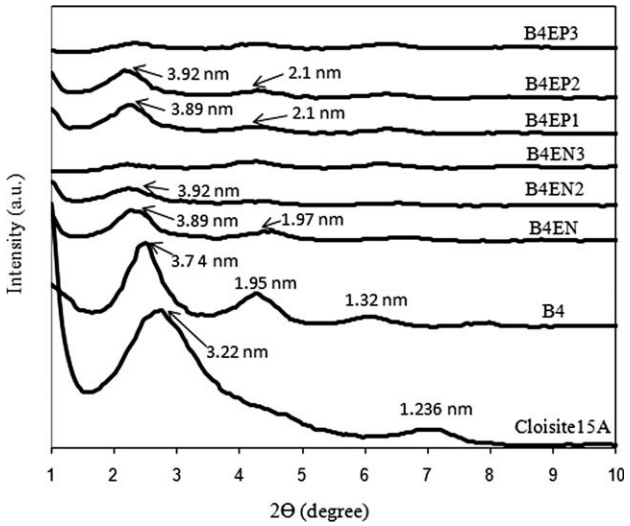

Figure 1 X-ray diffraction patterns of the neat organoclay (Cloisite 15A), uncompatibilized NR/SBR/OC (B4), and NR/SBR/OC nanocomposites compatibilized with EPDM-g-MAH and ENR50 with compatibilizer to clay ratio of 1, 2 and 3.

TEM images of uncompatibilized NR/SBR/OC composite (B4) are presented in Figure 2(a–c). The coexistence of intercalated nanoclay particles along with thin exfoliated nano platelets are clearly observed in the microstructure of compatibilized samples [Fig. 2(b,c)]. In these micrographs, NR and SBR phases are distinguished by two different colors and clay nanolayers are visible in both phases. One can clearly notice that the EPDM-*g*-MAH has had greater compatibilization effect in enhancing the clay interaction by the two rubber phases, leading to higher extent of intercalation/exfoliation and dispersion of the clay nano platelets. This is evidenced by higher elastic modulus exhibited by the B4EP3 nanocomposite vulcanizate as discussed in the following section.

Figure 3 displays the SEM images of the fractured surface morphology of the uncompatibilized NR/SBR/OC composite (B4), and their corresponding compatibilized (B4EN3, B4EP3) nanocomposites. These micrographs show that the failure of these samples follows different mechanisms. The uncompatibilized vulcanizate shows smooth fractured surface which is indicative of weak interface between the clay nano particles and polymer matrix which results in localized failure via delamination at the interface when the sample is cryo-fractured. But failure of the compatibilized vulcanizates is characterized by multiple crazing along different planes with virtually no failure at the particle–polymer interface [Fig. 3(b,c)]. In polymer-filler composites with enhanced interface, when a propagating crack meets the interface zones, it has to deviate in various directions which results in multiple failure planes and high roughness on the fractured surface. In another words, more roughness on the fractured surface is

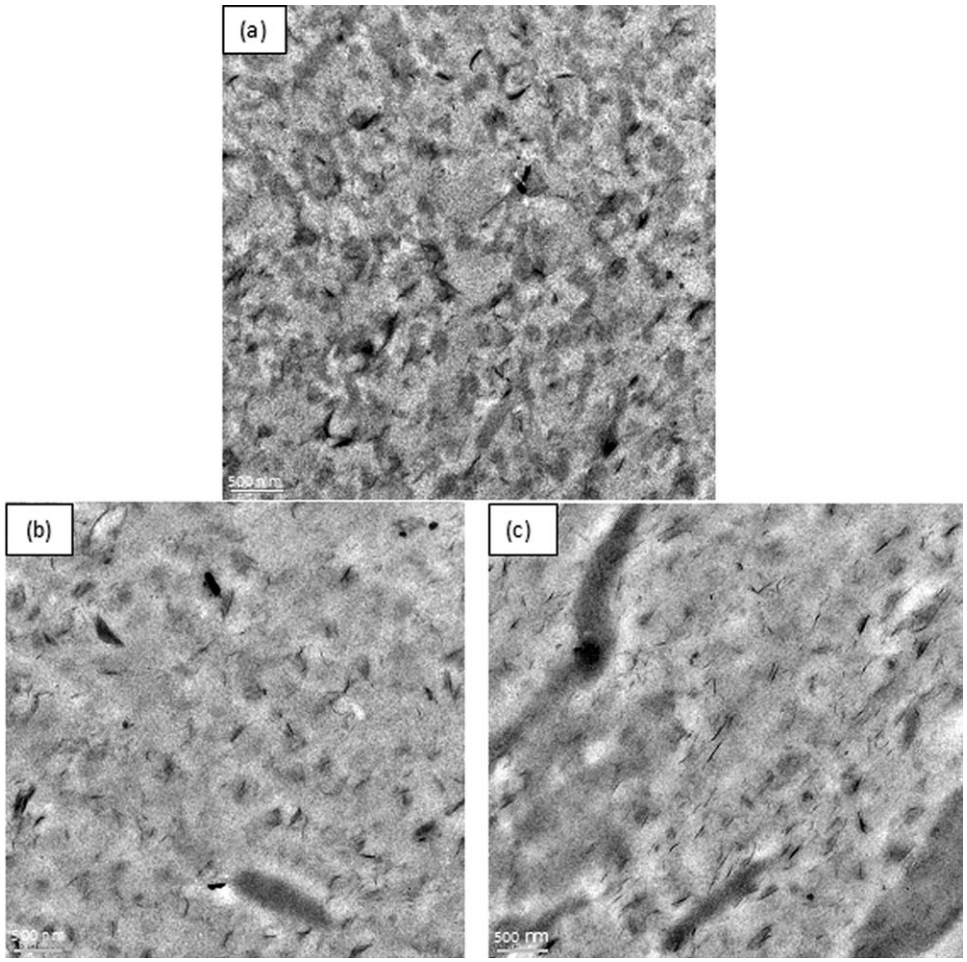

Figure 2 TEM micrographs of (a) uncompatibilized NR/SBR/OC (B4), and NR/SBR/OC nanocomposites compatibilized by: (b) ENR50 and, (c) EPDM-g-MAH with compatibilizer/clay ratio of 3.

indicative of greater resistance for the crack propagation due to better stress transfer from the rubber matrix to the nanoclay particles as a result of enhanced interfacial adhesion caused by the compatibilizer. Similar observations have also been reported by Pradhan et al.[48] for nanocomposites based on both EPDM and NBR rubbers.

To get further insight into the microstructure of the as-prepared blend composites, atomic force microscopy (AFM) in the tapping mode was performed on both uncompatibilized and compatibilized samples. In the tapping mode, the difference between the phase angle of the excitation signal and cantilever response was used to evaluate and map the variation in the blend composition, phase stiffness, and viscoelastic responses of the samples surface. Figure 4(a–c) displays the TMAFM 3D-images of the uncompatibilized and compatibilized NR/SBR/OC samples. The surface of uncompatibilized composite exhibited a non-rough surface with clay aggregates locally confined in various areas [Fig. 4(a)]. However, the histogram of the sectioned surface of the NR/SBR/OC nanocomposites generated by ENR50 and EPDM-*g*-MAH showed a rough surface [Fig. 4(b,c)]. The rough topography suggests the presence of various stiffened phases resulting from the enhanced interaction between rubber phases and clay nano platelets. The degree of surface roughness, in terms of mean roughness (R_a) and root mean square (R_q) values, for these samples was measured and quantified by the used AFM as have been displayed in Table II. It is clearly seen that the nanocomposite generated by EPDM-*g*-MAH (B4EP3) shows higher values of roughness, which evidences more stiffness for the rubber phase compared with the sample produced by ENR50 as compatibilizer and uncompatibilized vulcanizate. These results are consistent with the SEM micrographs discussed above.

Dynamic melt rheological behavior

Variation of melt complex viscosity (η*) and storage modulus (G') as a function of frequency obtained for the blend constituent (NR and SBR), and the nanocomposite samples based on the blend of these two elastomers are shown in Figures 5 and 6. As it can

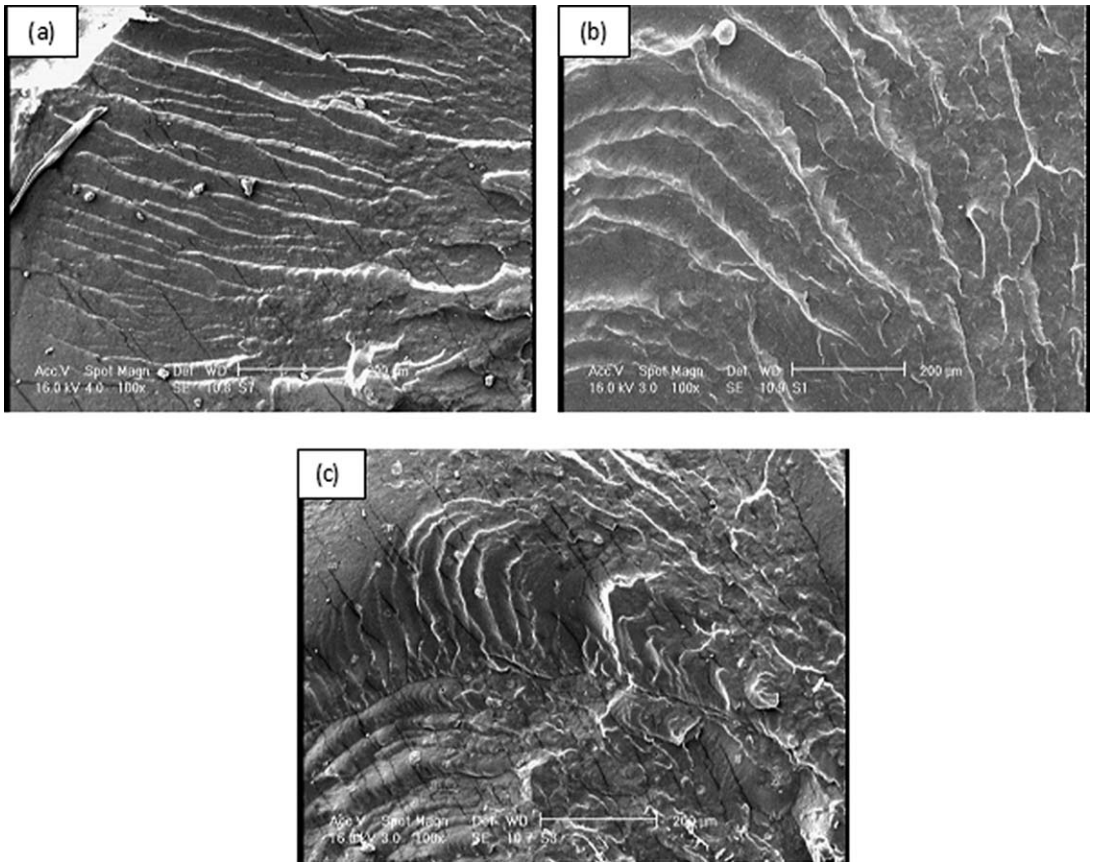

Figure 3 SEM micrographs of cryo-fractured surfaces, (a) uncompatibilized NR/SBR/OC (B4), and NR/SBR/OC nanocomposites compatibilized by: (b) ENR50 and (c) EPDM-*g*-MAH with compatibilizer/clay ratio of 3.

clearly be noticed the SBR exhibits much greater complex viscosity and storage modulus than NR, particularly within the low frequency region. It is also observed that the OC had more influence on increasing the complex viscosity and storage modulus of NR than that of SBR. These results suggest greater ability of NR for intercalation process. On the other hand, from a thermodynamic point of view, in a relatively non-polar rubber blend such as NR/SBR, the OC is expected to be located in both NR and SBR phases. Therefore, the lower increase of the melt viscosity of the SBR/OC nanocomposite sample by the clay platelets can mainly be attributed to higher melt elasticity (storage modulus) and therefore, lower ability of SBR chains to be involved in the melt intercalation process. This is evidenced by the melt viscoelastic behavior of NR/SBR/OC sample (Figs. 5 and 6) which suggests that nanoclay particles are mainly intercalated by the NR phase rather than SBR.

Figure 7 compares TEM micrographs of the simple blend sample (B) and the uncompatibilized blend nanocomposite (B4). The morphology of the unfilled blend seems to be semi-cocontinuous. This supports the results discussed above, suggesting that the OC is not selectively located in one of two phases. Otherwise, it would have caused a considerable change in the viscosity and melt elasticity ratios of the blend components, resulting in phase inversion (changing the morphology from semi-cocontinuous into matrix-disperse type).

Figures 8 and 9 show the linear melt viscoelastic behavior of the NR/SBR/OC nanocomposites generated by EPDM-*g*-MAH and ENR50 as compatibilizers. It can be observed that, both compatibilizers have had an enhancing effect on the dispersion of the clay nanoplatelets and their interaction with the rubber phases to make interconnected physical networks in the structure of the nanocomposites. This is evidenced by the pseudosolid-like behavior found within the low frequency region. However, it can be seen that EPDM-*g*-MAH has had higher reinforcing effect than ENR50. This effect monotonically increases with the compatibilizer content, so that a pronounced low frequency non-terminal storage modulus along with a viscosity upturn was exhibited at compatibilizer/clay ratios of 3.

Dynamic mechanical thermal analysis

To obtain further information on the extent of the rubber–OC interaction, and hence degree of restricted motions of the rubber segments, and also to learn more

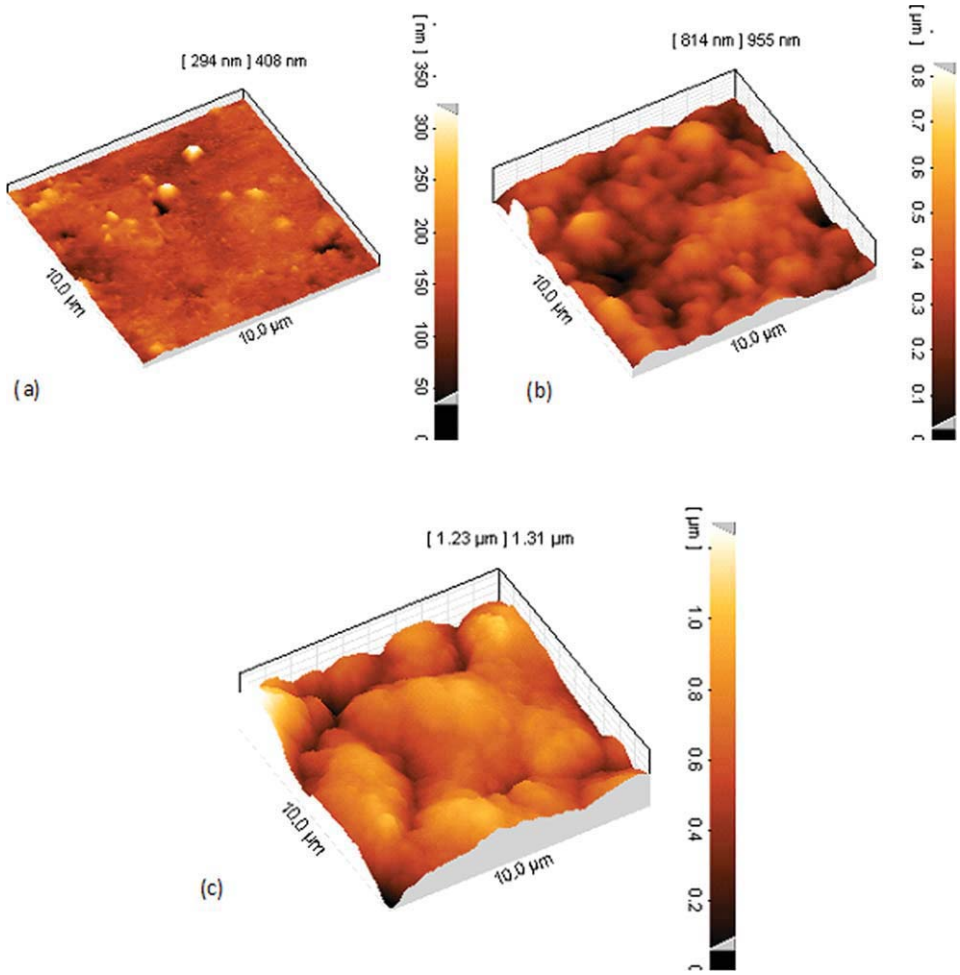

Figure 4 3-D images of (a) uncompatibilized NR/SBR/OC (B4) and NR/SBR/OC nanocomposites compatibilized by: (b) ENR50 and (c) EPDM-*g*-MAH with compatibilizer/clay ratio of 3. [Color figure can be viewed in the online issue, which is available at wileyonlinelibrary.com.]

on the effect of temperature on the mobility of the confined elastomer segments, DMTA was performed on the prepared nanocomposites. Figures 10 and 11 illustrate the dynamic storage modulus (E') and loss angle (tan δ) as a function of temperature (T) for different vulcanized samples. The values of storage modulus above the glass transition temperature were higher for the EPDM-*g*-MAH compatibilized NR/SBR/OC nanocomposite followed by the ENR50 compatibilized and uncompatibilized NR/SBR/OC vulcanizates (Fig. 10). These results are consistent with the higher degree of intercalation/exfoliation and hence greater contribution of OC in enhancing the stiffness of NR/SBR/OC nanocomposite samples compatibilized by EPDM-*g*-MAH. In Figure 11, the variation of damping factor (tan δ) versus temperature has been illustrated and compared for various samples. It is clearly seen that,

TABLE II
Quantitative Parameters of Nanocomposites

Sample code	RMS (R_q) (nm)	R_a (nm)
B4	24.9	16.9
B4EN3	94	73.1
B4EP3	161	126

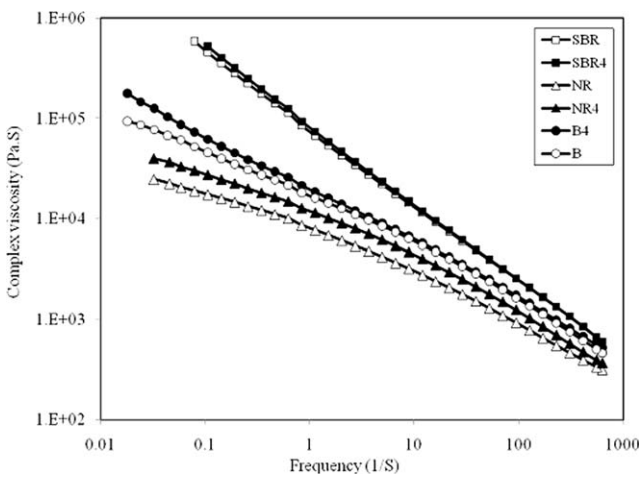

Figure 5 Complex viscosity (η*) as a function of frequency (ω) for unfilled NR, SBR, simple blend of NR/SBR, and filled counterparts.

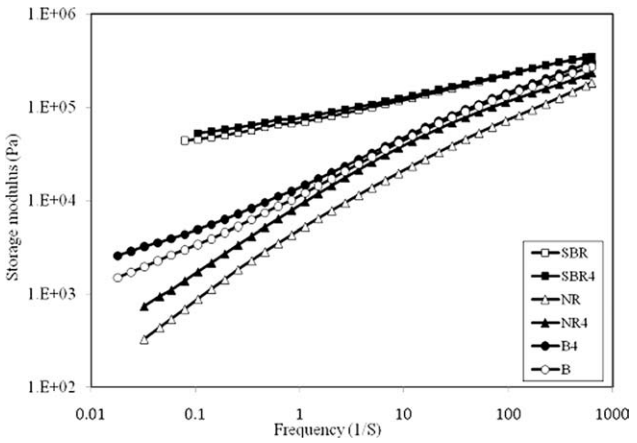

Figure 6 Melt shear storage modulus (G') as a function of frequency (ω) for unfilled NR, SBR, simple blend of NR/SBR, and filled counterparts.

the height of the tan δ_{max} has decreased for both compatibilized nanocomposite vulcanizates. However, reduction in the height of tan δ_{max} showed to be higher when the compatibilizer/clay ratio was raised to the value of 3 for both compatibilized samples. This evidences the intensification of the interface between the clay silicate layers and the rubber segments, and hence the freezing effect of the viscous motions of the chains confined within the clay networks. The reduced tan δ_{max} for the compatibilized nanocomposites under low strain amplitude during DMTA analysis also suggests the presence of clay physical networks which resist the break down when subjected to short range strain amplitude. However, all the blend nanocomposites generated from ENR50 exhibit a second viscoelastic transition above the glass transition temperature. This has been suggested to be due to the time-dependent motions of the pendent epoxy groups in the structure of ENR50.[31] Moreover, as can be observed, tan δ_{max} of the compatibilized blend nanocomposites show a slight shift to a higher temperature, indicating more restricted motions for the segments of both rubber phases. As the glass transition temperature of NR and SBR phases are overlapped, it is hard to make any conclusion on the difference in partitioning of silicate layers between the phases. The lower tan δ_{max} for both NR/SBR/clay compatibilized nanocomposites is also indicative of the low strain amplitude resistance of the clay networks, and hence the lower possibility for the clay nanolayers to undergo reorientation under the applied dynamic forces. Occurrence of reorientation by the anisotropic dispersed nanolayers has been suggested as the main cause of mechanical damping by polymer/clay nanocomposites.[49]

Curing characterization

Table III illustrates the measured curing characteristics of the prepared compounds. It is clearly observed that inclusion of OC into the blend compound has led to the reduction of the scorch time and acceleration of the cure rate. This is attributed to the activating effects of the surfactant in the structure of the used OC.[12,50]

However, the scorch time and curing rate of the unfilled compatibilized compounds containing either ENR50 or EPDM-*g*-MAH did not show significant change compared to the unfilled simple blend sample (B), indicating that neither EPDM-*g*-MAH nor ENR50 affects the curing behavior of the compounded blend. Moreover, the difference between maximum and minimum torque ($M_H - M_L$), which has a direct relation with the extent of crosslink density,[41] was comparable for the two NR/SBR/OC nanocomposites generated by ENR50 and EPDM-*g*-MAH as compatibilizer.

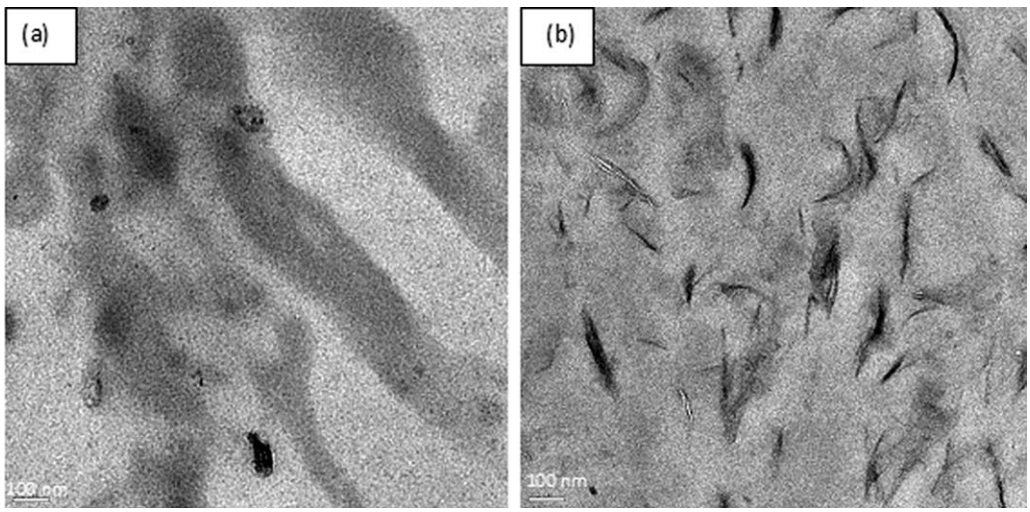

Figure 7 TEM micrographs of (a) unfilled NR/SBR simple blend (B) and (b) uncompatibilized NR/SBR/OC vulcanizate (B4).

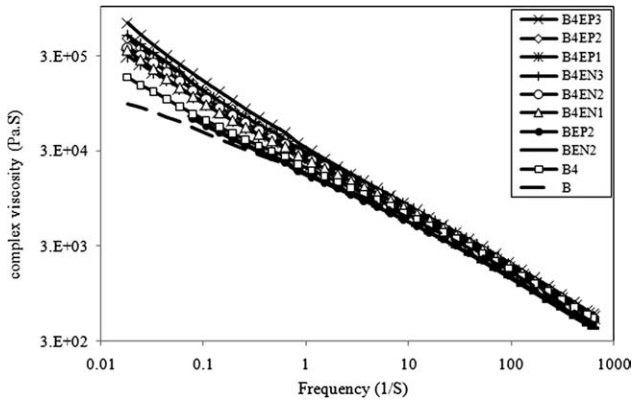

Figure 8 Melt complex viscosity (η*) as a function of frequency (ω) for the NR/SBR simple blend (B), unfilled NR/SBR blend but containing compatibilizer (BEP2, BEN2), uncompatibilized NR/SBR/OC composite (B4), and NR/SBR/OC nanocomposites generated by EPDM-g-MAH and ENR50 with compatibilizer to clay ratio of 1, 2 and 3.

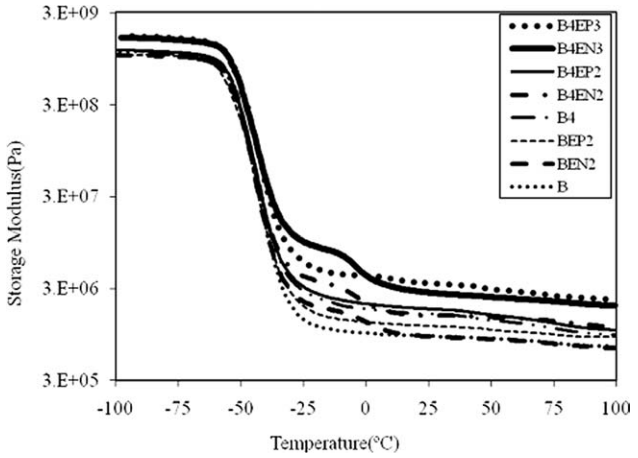

Figure 10 Storage modulus (E′) as a function of temperature (T) for NR/SBR simple blend (B), unfilled NR/SBR blend but containing compatibilizer (BEP2, BEN2), uncompatibilized NR/SBR/OC sample (B4), and NR/SBR/OC nanocomposites generated by EPDM-g-MAH and ENR50 with compatibilizer to clay ratio of 2 and 3.

Tensile properties

Tensile behavior of polymer–clay nanocomposite vulcanizates depends on several factors, including the extent of clay dispersion, the degree of interfacial adhesion between the clay platelets and the polymer matrix as well as the extent of crosslink density.[35] To correlate the macromechanical properties with the microstructure of the prepared NR/SBR/OC nanocomposites, tensile properties of the prepared vulcanized nanocomposites were evaluated as demonstrated in Figures 12(a,b) and 13. It is clearly seen that both compatibilized nanocomposites originated from ENR50 and EPDM-*g*-MAH as compatibilizer exhibited enhanced strength as well as stress at 100 and 300% elongation in comparison with the neat and uncompatibilized filled NR/SBR vulcanizates. However, the extent of reinforcement was distinct for the nanocomposites generated by the two compatibilizers when compatibilizer to clay ratio was increased to 3 (B4EP3 and B4EN3). These are consistent with the formation of more polymer–clay interaction sites, and also higher surface roughness factor exhibited by the cryo-fractured surfaces of these samples, which could be attributed to the reinforced interactions between the rubber phases and clay nanolayers. Comparing the tensile mechanical behavior of the NR/SBR blend nanocomposite originated by EPDM-*g*-MAH with those prepared by

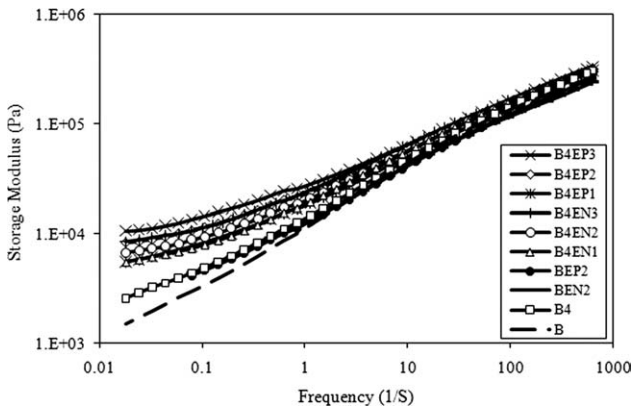

Figure 9 Melt shear storage modulus (G′) as a function of frequency (ω) for the NR/SBR simple blend (B), unfilled NR/SBR blend but containing compatibilizer (BEP2, BEN2), uncompatibilized NR/SBR/OC sample (B4), and NR/SBR/OC nanocomposites based on EPDM-g-MAH and ENR50 with compatibilizer to clay ratio of 1, 2 and 3.

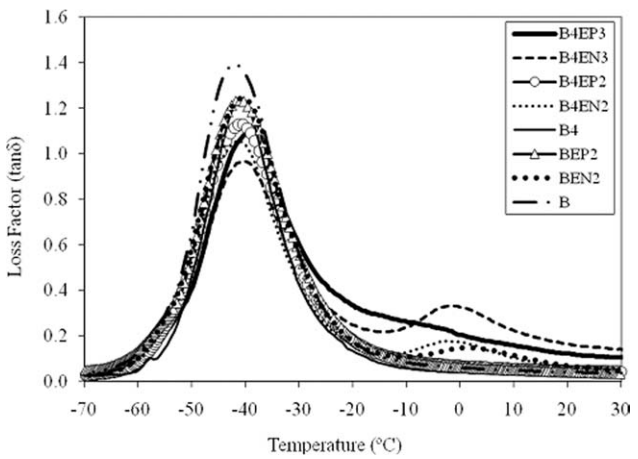

Figure 11 Dynamic loss factor (tan δ) as a function of temperature (*T*) for NR/SBR simple blend (B), unfilled NR/SBR blend but containing compatibilizer (BEP2, BEN2), uncompatibilized NR/SBR/OC sample (B4), and NR/SBR/OC nanocomposites based on EPDM-*g*-MAH and ENR50 with compatibilizer to clay ratio of 2 and 3.

TABLE III
Curing Characteristics of the Prepared Compounds

Sample code	t_2 (sec)	t_{90} (sec)	M_H (dN m)	M_L (dN m)	$M_H - M_L$ (dN m)	CRI (min^{-1})
B	495	1055	12.62	0.83	11.79	10.71
B4	207	551	12.69	0.93	11.79	17.44
B4EN1	187	534	13.38	0.9	12.48	17.29
B4EN2	157	468	13.93	0.9	13.03	19.29
B4EN3	157	434	13.93	0.91	13.02	21.66
B4EP1	220	674	13.59	0.97	12.62	13.22
B4EP2	207	610	14.28	1.03	13.25	14.89
B4EP3	212	541	14.35	1.03	13.32	18.24
BEN2	473	1009	12.62	0.9	11.72	11.19
BEP2	548	1119	12.66	0.9	11.76	10.51

ENR50 suggests more effectiveness of EPDM-*g*-MAH as compatibilizer in reinforcing the NR/SBR/OC nanocomposites. As the crosslink densities ($M_H - M_L$) of the two compatibilized nanocomposite vulcanizates were found to be comparable, the increased tensile strength observed for the B4EP3 sample reveals the higher enhancement of interfacial interactions between the clay nanolayers and the rubber phases by EPDM-*g*-MAH.

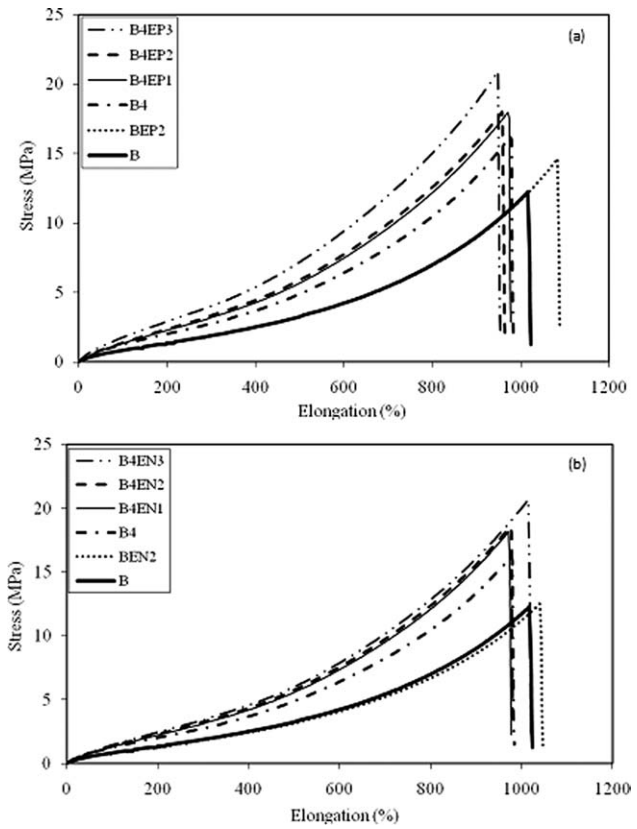

Figure 12 Tensile strength and elongation at break for the NR/SBR simple blend (B), unfilled NR/SBR blend but containing compatibilizer (BEP2, BEN2), uncompatibilized NR/SBR/OC sample (B4), and NR/SBR/OC nanocomposites compatibilized by: (a) EPDM-g-MAH and (b) ENR50 with compatibilizer to clay ratio of 1, 2 and 3.

Fatigue life and dynamic heat generation

The fatigue life is closely related to the crack growth characteristics of materials. Fatigue occurs in some cases as a result of the propagation of unstable cracks or defects under the applied cyclic forces. All rubber vulcanizates have viscoelastic characteristics which results in an energy loss when subjected to a long cyclic deformation, which is called dynamic hysteresis. Hysteresis or energy loss leads to the increase of the sample temperature during the period which is under cyclic stress fields. However, energy loss has been shown to increase the fatigue resistance of the rubber vulcanizate due to the retardation of crack growth.[51] In polymer/OC nanocomposites, the intercalated polymer segments may be able to undergo slippage between the nanolayers or on the surface of OC particles when a cyclic force is applied. The rubber/clay intercalated structures can be considered as a physical network. Therefore, deformation of such physical networks together with chain slippage allow more frictional energy

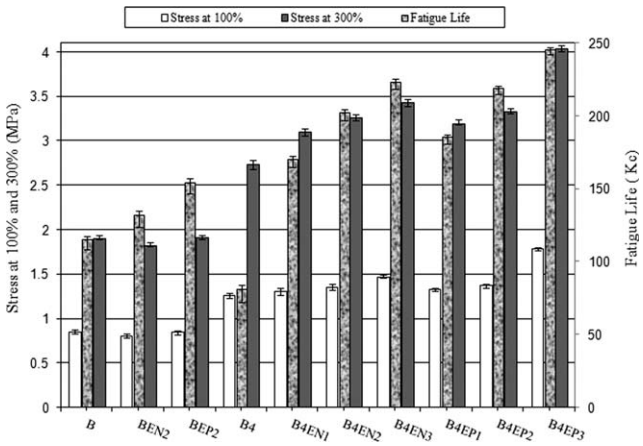

Figure 13 Stress at 100%, 300% elongation and fatigue life for the NR/SBR simple blend (B), unfilled NR/SBR blend but containing compatibilizer (BEP2, BEN2), uncompatibilized NR/SBR/OC composite (B4), and NR/SBR/OC nanocomposites generated by EPDM-g-MAH and ENR50 with compatibilizer to clay ratio of 1, 2 and 3.

TABLE IV
Heat Build-up of Prepared Samples

Sample code	Increase in temperature (°C)
B	17.8
B4	19.8
B4EN3	24.4
B4EP3	29.8

dissipation which leads to the prevention of localized stress concentration, and hence retardation of crack growth. The relationship between fatigue life and extent of hysteresis behavior has also been reported for SBR vulcanizates reinforced by carbon black.[52] Heat build-up has also been related to hysteresis loss in filled rubber composites.[53] The measured fatigue life and heat build-up for the prepared compounds have been illustrated in Figure 13 and Table IV. The highest fatigue life of B4EP3 nanocomposite vulcanizate compared with B4EN3 is consistent with its highest hysteresis as shown in Table IV. This might be related to the higher extent of intercalated and/or exfoliated structure together with a more enhanced interfacial interaction between the rubber phases and the clay nanolayers when EPDM-*g*-MAH was incorporated as compatibilizer. In another words, stronger interphase can result in better stress transfer from the matrix to the filler, and therefore enhancement of fatigue life. Moreover, the uncompatibilized NR/SBR/OC (B4) composite shows lower fatigue life than the neat blend of rubbers (B), which can be attributed to lack of compatibility between the rubber phases and the nanoclay, and therefore unsuitable dispersion of the OC and agglomeration formation of nanolayers in the matrix [Fig. 2(a)] that lead to stress concentration in cyclic deformations.

CONCLUSIONS

NR/SBR (70/30)/OC nanocomposites were successfully prepared by melt-mixing process. To improve the clay dispersion and also compatibility between the two rubber phases and the OC particles, two different interfacial compatibilizers including maleated EPDM rubber (EPDM-*g*-MAH) and epoxidized NR (ENR50) were employed. The influence of EPDM-*g*-MAH and ENR50 in enhancing interfacial interaction between OC nanolayers and NR and SBR phases, and hence their influence in the developed microstructure were evaluated and compared. All examinations not only showed better dispersion of the clay nanolayers in the structure of the interfacially compatibilized nanocomposites, but also the original semi-cocontinuous morphology for the two rubber phases was found to be retained, suggesting similar affinity of the two phases towards the clay particles.

Based on the results obtained, it is concluded that nanocomposites originating from EPDM-*g*-MAH as compatibilizer, especially at compatibilizer/clay ratios of 3, exhibited the highest interaction between the rubber phases and the OC particles, and hence better mechano-dynamic properties than the counterpart samples prepared by ENR50 as compatibilizer. Both XRD and TEM examinations verified that the two rubber phases of the rubber blend compatibilized by both EPDM-*g*-MAH and ENR50 could be intercalated into the galleries of OC and high extent of clay intercalation/exfoliation could be obtained in these nanocomposites. This is evidenced by the high melt dynamic viscosity and more pseudosolid-like behavior exhibited within low frequency region by the two interfacially compatibilized NR/SBR/OC nanocomposites. Higher degree of the clay nanolayers dispersion along with their intensified interfacial interactions with the two rubber phases in the structure of the compatibilized nanocomposites were confirmed by more reinforcement of tensile strength together with higher stress at 100 and 300% elongation for the two interfacially compatibilized nanocomposite vulcanizates compared with the clay filled but uncompatibilized sample. Lower mechanical damping for the two compatibilized NR/SBR/OC nanocomposites suggested more restricted motions for the NR and SBR segments in vicinity of the clay nanolayers. The two interfacially compatibilized NR/SBR/OC nanocomposites exhibited enhanced fatigue life which was consistent with their higher dynamic hysteresis under large strain cyclic deformations. Nanocomposite vulcanizates originated by EPDM-*g*-MAH as compatibilizer showed more hysteresis and also higher fatigue life compared with the vulcanizate of the nanocomposite originated by ENR50 as compatibilizer.

The authors thank Mr. Mustafa Guler from Institute of Materials Science and Nanotechnology, Bilkent University, for preparing TEM samples and also TEM measurements.

References

1. Frogley, M. D.; Ravish, D.; Wagner, H. D. Compos Sci Technol 2003, 63, 1647.
2. Biswas, M.; Ray, S. S. Adv Polym Sci 2000, 155, 167.
3. Lebaron, P. C.; Wang, Z.; Pinnavaia, T. Appl Clay Sci 1999, 15, 11.
4. Kojima, Y.; Usuki, A.; Kawasumi, M. Okada, A.; Kurauchi, T.; Kamigaito, O. J Appl Polym Sci 1993, 49, 1259.
5. Ray, S. S.; Okamoto, M. Prog Polym Sci 2003, 28, 1539.
6. Paul, D. R.; Robenson, L. M. Polymer 2008, 49, 3187.
7. Giannelis, E. P.; Krishnamoorti, R.; Manias, E. Adv Polym Sci 1999, 138, 107.
8. Lopez-Manchado, M. A.; Herrero, B.; Arroyo, M. Polym Int 2003, 52, 1070.
9. Vaia, R. A.; Giannelis, E. P. Macromolecules 1997, 30, 8000.

10. Ma, Y.; Wu, Y. P.; Zhang, L. Q.; Li, Q. F. J Appl Polym Sci 2008, 109, 1925.
11. Lopez-Manchado, M. A.; Arroyo, M.; Herrero, B. J Appl Polym Sci 2003, 89, 1.
12. Arroyo, M.; Lopez-Manchado, M. A.; Herrero, B. 2003, 44, 2447.
13. Bousmina, M. Macromolecules 2006, 39, 4259.
14. Dennis, H. R.; Hunter, D. L.; Chang, D.; Kim, S. Polymer 2001, 42, 9513.
15. Homminga, D.; Goderis, B.; Hoffman, S.; Reynaers, H. Polymer 2005, 46, 9941.
16. Drumright, R. E.; Gruber, P. R.; Henton, D. E. Adv Mater 2000, 12, 1841.
17. Krause, S.; Goh, S. H. In Polymer Handbook; Brandrup, J., Immergut, E. H., Grulke, E. A., Eds., Wiley: New York, 1999, 409.
18. Datta, S.; Lehse, D. J. Polymer Compatibilizers; Hanser: Munich, 1996.
19. Gatos, K. G.; Thomann, R.; Karger-Kocsis, J. Polym Int 2004, 53, 1191.
20. Sadhu, S.; Bhowmick, A. K. J Mater Sci 2005, 40, 1633.
21. Wang, X. P.; Huang, A. M.; Jia, D. M.; Li, Y. M. Eur Polym Mater 2008, 44, 2784.
22. Sadhu, S.; Bhowmick, A. K. Rubber Chem Technol 2003, 76, 860.
23. Ganter, M.; Gronski, W.; Reichert, P.; Mulhaupt, R. Rubber Chem Technol 2001, 74, 221.
24. Sadhu, S.; Bhowmick, A. K. J Appl Polym Sci 2004, 92, 698.
25. Madhusoodanan, K. N.; Varghese, S. J Appl Polym Sci 2006, 102, 2537.
26. Song, M.; Wong, C. W.; Jin, J.; Ansarifar, A. Polym Int 2005, 54, 560.
27. Vaia, R. A.; Jandt, K. D.; Kramer, E. J.; Giannelis, E. P. Macromolecules 1995, 28, 8080.
28. Essawy, H.; El-Nashar, D. Polym Test 2004, 23, 803.
29. Stephen, R.; Varghese, S.; Joseph, K.; Oommen, Z.; Thomas, S. J Membr Sci 2006, 282, 162.
30. Stephen, R.; Alex, R.; Cherian, T.; Varghese, S.; Joseph, K.; Thomas, S. J Appl Polym Sci 2006, 101, 2355.
31. Arroyo, M.; López-Manchado, M. A.; Valentin, J. L.; Carretero, J. Compos Sci Technol 2007, 67, 1330.
32. Bandyopadhayay, A.; Thakur, V.; Pradhan, S.; Bhowmick, A. K. J Appl Polym Sci 2010, 115, 1237.
33. Ray, S. S.; Bousmina, M. Polym Eng Sci 2006, 46, 1121.
34. Ramorino, G.; Bignotti, F.; Conzatti, L.; Ricco, T. Polym Eng Sci 2007, 47, 1650.
35. Pal, K.; Rajasekar, R.; Kang, D. J.; Zhang, Z. X.; Pal, S. K. Mater Design 2010, 31, 677.
36. Carretero-Gonzalez, J.; Retsos, H.; Verdejo, R.; Toki, S.; Hsiao, B. S.; Giannelis, E. P.; Lopez-Manchado, M. A. Macromolecules 2008, 41, 6763.
37. Gu, Z.; Song, G.; Liu, W.; Li, P.; Gao, L.; Li, H.; Hu, X. Appl Clay Sci 2009, 46, 241.
38. Rahmatpour, A.; Abdollahi, M.; Shojaee, M. J Macromol Sci Part B Phys 2008, 47, 523.
39. Sadhu, S.; Bhowmick, A. K. Adv Eng Mater 2004, 6, 738.
40. Chakraborty, S.; Kar, S.; Dasgupta, S.; Mukhopadhyay, R.; Bandyopadhyay, S.; Joshi, M.; Ameta, S. C. Polym Test 2010, 29, 181.
41. Teh, P. L.; Mohd-Ishak, Z. A.; Hashim, A. S.; Karger-Kocsis, J. Eur Polym J 2004, 40, 2513.
42. Teh, P. L.; Mohd-Ishak, Z. A.; Hashim, A. S.; Karger-Kocsis, J.; Ishiaku, U. S. J Appl Polym Sci 2004, 94, 2438.
43. Teh, P. L.; Mohd-Ishak, Z. A.; Hashim, A. S.; Karger-Kocsis, J.; Ishiaku, U. S. J Appl Polym Sci 2006, 100, 1083.
44. Rajasekar, R.; Pal, K.; Zheng, P.; Ying, C.; Das, C. K. Compos Sci Technol 2008, 4, 17.
45. Tavakoli, M.; Katbab, A. A.; Nazockdast, H. J. Macromol Sci Part B Phys 2011, 50, 1.
46. Ganguly, A.; Bhowmick, A. K. J Appl Polym Sci 2009, 111, 2104.
47. Poh, B. T.; Ismail, H.; Quah, E. H.; Chin, P. L. J Appl Polym Sci 2001, 81, 47.
48. Pradhan, S.; Costa, F. R.; Wagenknecht, U.; Jehnichen, D.; Bhowmick, A. K.; Heinrich, G. Eur Polym Mater 2008, 44, 3122.
49. Ganter, M.; Gronski, W.; Semke, H.; Zilg, T.; Thomann, C.; Muhlhaupt, R. Kautschuk Gummi Kunststoffe 2001, 54, 166.
50. Varghese, S.; Karger-Kocsis, J.; Gatos, K. G. Polymer 2003, 44, 3977.
51. Gatos, K. G.; Sawanis, N. S.; Apostolov, A. A.; Thomann, R.; Karger-Kocsis, J. Macromol Mater Eng 2004, 289, 1079.
52. Wu, Y.; Zhao, W.; Zhang, L. Q. Macromol Mater Eng 2006, 291, 944.
53. Kar, K. K.; Bhowmick, A. K. J Appl Polym Sci 1997, 64, 1541.